Materials Transactions, Vol. 49, No. 10 (2008) pp. 2315 to 2321

Effects of Vacancies on Deformation Behavior in Nanocrystalline Nickel

Motohiro Yuasa[1,*1], Hiroshi Matsumoto[1,*2], Masataka Hakamada[2] and Mamoru Mabuchi[1]

[1]*Department of Energy Science and Technology, Graduate School of Energy Science, Kyoto University, Kyoto 606-8501, Japan*
[2]*Materials Research Institute for Sustainable Development, National Institute of Advanced Industrial Science and Technology, Nagoya 463-8560, Japan*

The effects of vacancies on deformation of nanocrystalline Ni have been investigated by experiments and molecular dynamics (MD) simulations. In the experiments, nanocrystalline Ni specimens containing different numbers of vacancies were produced by electrodeposition and annealing, and their mechanical properties were investigated by tensile tests. As a result, the yield stress and fracture stress for the specimen containing more vacancies were lower than those for the one containing fewer vacancies. The MD simulations showed that the grain boundary energy is increased by the presence of vacancies in the grain boundary, however, that an increase in grain boundary energy with straining is reduced by the presence of vacancies in the grain boundary. The results of the experiments and simulations suggested that there is a correlation between the grain boundary energy characteristics and the mechanical properties of the nanocrystalline Ni.
[doi:10.2320/matertrans.MRA2008115]

(Received April 4, 2008; Accepted July 2, 2008; Published August 13, 2008)

Keywords: *nanocrystalline metal, electrodeposition, mechanical properties, molecular dynamics simulation, vacancy*

1. Introduction

Nanocrystalline materials[1–6] have been the subject of widespread research over the past couple of decades. It is well known that the grain size has a significant effect on the mechanical behavior of metallic materials such as the yield stress and flow stress. The relationship between the yield stress, σ_y, and the grain size, d, can be given by the Hall-Petch relation:[7,8]

$$\sigma_y = \sigma_0 + kd^{-1/2} \quad (1)$$

where σ_0 is the friction stress required to move individual dislocations (or the yield stress of a single crystal) and k is a constant, called the Hall-Petch intensity parameter.[8] However, as the grain size is reduced to nanometer-scale, the Hall-Petch relation breaks down and a peculiar phenomenon called the "inverse Hall-Petch effect",[9–11] that is, a decrease in yield stress with decreasing grain size occurs. Investigations via experiments[12,13] and molecular dynamics (MD) simulations[14–16] revealed that the critical grain size below which the inverse Hall-Petch effect holds is approximately 10 nm and that the plastic deformation in this region is mainly due to the grain boundary process.

For nanocrystalline metals whose grain size is below a critical grain size, because their dominant deformation process is a grain-boundary-based process such as grain boundary sliding, grain boundary properties are suggested to strongly affect the deformation and fracture characteristics of a nanocrystalline metal. MD simulations[17–19] showed that the mechanical properties of a nanocrystalline metal are affected by porosity and structural disorder in the grain boundary. Recently, Fukai *et al.*[20] reported that metals produced by electrodeposition have an excess number of vacancies. This indicates that the mechanical properties of a nanocrystalline metal produced by electrodeposition are strongly affected by vacancies. Therefore, it is important to understand the roles of vacancies in deformation of a nanocrystalline metal produced by electrodeposition.

Molecular dynamics (MD) simulations have played a vital role for understanding of deformation mechanisms in nanocrystalline materials.[14,21,22] Moreover, the combined use of experiments and simulations is desirable for deeper comprehension. In the present paper, tensile tests and MD simulations are conducted to investigate the effects of vacancies on deformation of nanocrystalline nickel produced by electrodeposition. In the experimental investigation, tensile properties of a nanocrystalline Ni-W film containing more vacancies are compared with those of one containing fewer vacancies. Also, MD simulation is carried out to analyze the role of vacancies from the viewpoint of the atomic level. In particular, the grain boundary energy, which is one of the critical grain boundary properties, is focused, because it is affected by the presence of vacancies in the grain boundary.[23] On the basis of the results of tensile tests and MD simulations, the relationship between the grain boundary energy and deformation characteristics in nanocrystalline Ni is discussed.

2. Experimental and Simulation Procedures

2.1 Experimental

A nanocrystalline Ni-22 mass%W film was produced by electrodeposition. Ductility is often reduced by internal flaws in nanocrystalline metals.[24] However, nanocrystalline Ni without flaws can be obtained by electrodeposition. The chemical composition of a plating bath and electrodeposition conditions for producing a nanocrystalline Ni-W film are listed in Tables 1 and 2, respectively. Under these conditions, the Ni-W films whose thickness was 20 μm were deposited on a Cu substrate.

The grain boundary structure of a nanocrystalline metal can be changed by annealing.[18] In the present investigation, annealing was carried out on the Ni films at a relatively low temperature of 353 K to suppress grain growth: specimen A was annealed at 353 K for 24 hours in vacuum, and specimen B was annealed at 353 K for 48 hours in vacuum. The

*1Graduate Student, Kyoto University
*2Graduate Student, Kyoto University. Present address: Tokyo Electric Power Comapany, Tokyo 100-8560, Japan

Table 1 Chemical composition of a plating bath for producing nanocrystalline Ni-W films.

Chemicals	Concentration, c/mol/l
$NiSO_4$-$6H_2O$	0.06
$Na_3C_6H_5O_7$-$2H_2O$	0.25
Na_2WO_4-$2H_2O$	0.14
$(NH_4)_2SO_4$	0.25
$(CH_3)(CH_2)_{10}CH_2OSO_3Na$	0.0017

Table 2 Operating conditions of electrodeposition for producing nanocrystalline Ni-W films.

Parameters	
Plating temperature (K)	333
Current density (A/cm^2)	0.05
pH	7.5
Anode material	Pt
Substrate	Cu

microstructures of the nanocrystalline Ni films were observed by high-resolution transmission electron microscopy (HRTEM). The specimens for HRTEM observation were prepared by polishing the specimens with an ion milling device prior to conducting tensile tests. To investigate the number of vacancies in both specimens, positron lifetime measurements (PLMs)[25] were performed using a conventional lifetime spectrometer with a resolution of about 290 ps. The positron source was $_{22}$NaCl (about 1.85 MBq) and all the spectra contained more than 2×10^6 counts.

Four samples on each specimen were cut by an electric discharge machine for tensile tests. The dimensions of the samples were 8 mm in gage length, 2 mm in gage width and 20 mm in gage thickness, respectively. Tensile tests were conducted at room temperature using an INSTRON-type tensile testing machine.

2.2 Molecular dynamics simulation

MD simulations were carried out using a two-dimensional (2D) columnar nanocrystalline Ni cell unit. Atomic and dislocation events taking place during deformation can be monitored by MD simulation with a 2D columnar cell unit,[26–29] although there is a difference in the level of dislocation activity between 2D columnar and 3D nanocrystalline structures.[30] MD simulation with a 2D columnar cell unit permits the investigation of specimens much larger grain sizes and with a constant microstructure.[26] The cell unit used in the present paper consisted of four columnar, uniform hexagonal fcc grains that were rotated around the [100] axis, which was defined as the x direction, to suppress the activity of dislocations. The misorientation angles of grain boundaries in the unit cell were set to be 22.5, 45, and 67.5 degrees; consequently, the cell had 12 tilt grain boundaries. The dimensions of the cell are 1.06, 5.97 and 6.27 nm. A relaxation calculation was carried out for 20 ps at a constant temperature (= 300 K) and at a constant pressure (= 1 atm), with the 3D periodic boundary condition and the NTP ensemble. This cell unit is called the normal cell unit in the present paper. The grain size in the cell unit was about 3 nm. The critical grain sizes below which the inverse Hall-Petch effect holds in Ni have been obtained to be 7–9 nm from hardness tests[12] and about 10 nm from MD simulation.[21] Thus, the grain size in the cell unit of 3 nm size is smaller than the critical grain size. Farkas and Curtin[26] showed that there is no inverse Hall-Petch effect beyond the grain size range of 4–20 nm in MD simulation with a 2D columnar cell unit. In the present work, however, a preliminary MD simulation was performed using same-shaped cell units with different grain sizes; as a result, the flow stress decreased with decreasing grain size. Hence, it has been verified that the MD simulation with the 2D columnar cell unit in the present work can be used.

To investigate the effects of vacancies on the deformation characteristics of a nanocrystalline Ni, another cell unit was used by removing one atom from each grain boundary in the normal cell unit. As a result, a total of 12 atoms were removed from a cell unit. After removing the atoms, relaxation calculation was carried out by the same condition as the normal cell relaxation. It was verified from stability of the total internal energy by extended relaxation calculations that the relaxation was enough for stabilizing the grain boundary structure. The cell unit after removing 12 atoms at grain boundaries is called the vacancy-rich cell unit in the present paper.

MD creep test simulations were carried out at a constant temperature (= 300 K) and at a constant pressure (= 1 atm), using an EAM potential (Rosato-Guillope-Legrand-type (RGL) potential[31]), which is applicable to Ni, with the 3D periodic boundary condition and the NTP ensemble. In the simulation, the time step was 1 fs, the temperature control was realized using the scaling approach (the scaling interval was 1 time step) and the cutoff distance was 0.553 nm. In the creep test simulation, a constant tensile stress of 2.53 GPa was applied in the z direction for 15 ps (15000 steps).

Next, compression test simulations were performed to investigate the relationship between the deformation characteristics and the grain boundary energy. On the other hand, in tensile test simulations, cracks were formed in conjunction with the onset of plastic deformation, and tensile test simulations were not carried out for the investigation. The simulations were carried out at a constant temperature (= 300 K) and at a constant volume, using the RGL potential, with the 3D periodic boundary condition and the NTV ensemble. The conditions of the time step, temperature control and cutoff distance were the same as those in the above creep simulations. In the compression test simulations, the cell units were compressed in the z direction by 1%, where the simulation time for compression by 1% was 20 ps (namely, the strain rate was 5×10^8 s^{-1}), and the z-direction stress and grain boundary energy were monitored. The compressive deformation was simulated until 9% compressive strain by repeating compression by 1% strain.

3. Results

3.1 Microstructures

The microstructures of specimens A and B examined by HRTEM are shown in Fig. 1. Flaws and pores with sizes on the order of nanometers and above were not observed in both

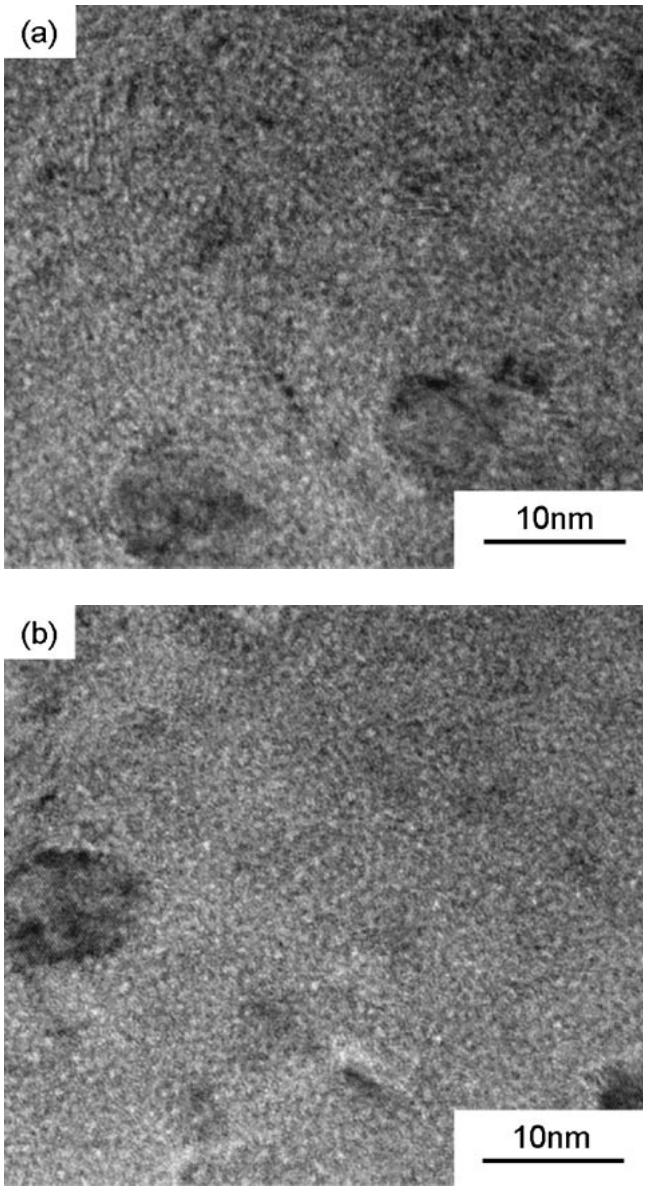

Fig. 1 High-resolution transmission electron microscopic images of the nanocrystalline Ni alloy produced by electrodeposition, (a) specimen A and (b) specimen B.

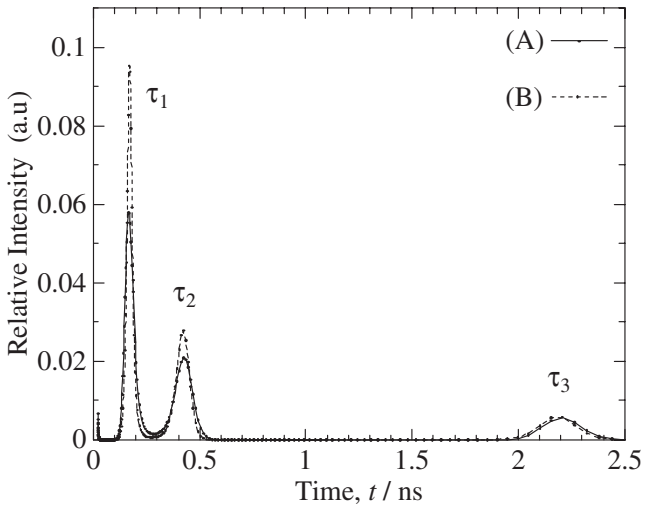

Fig. 2 Positron lifetime distribution curves of specimen A, which is shown with a full line (A), and specimen B, which is shown with a dotted line (B), where τ_1 (150–200 ps), τ_2 (400–450 ps), and τ_3 (2000–2500 ps) are the peaks of positron lifetime.

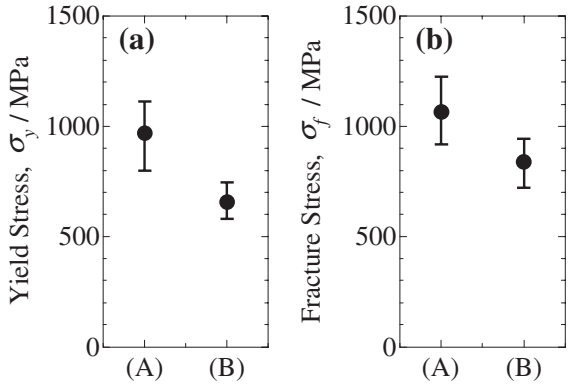

Fig. 3 Yield stress and fracture stress of specimens A and B by tensile tests at room temperature, where a filled circle is an average.

specimens. The mean grain size of specimen A determined from HRTEM observation was 6.5 nm and that of specimen B was 6.7 nm. Also, from X-ray diffraction measurements, the grain size calculated by the Scherrer equation was 2.0 nm for the specimen A and 2.2 nm for the specimen B, respectively. The critical grain size below which the inverse Hall-Petch effect holds in Ni is 7–10 nm.[12,21] Thus, the nanocrystalline Ni produced in the present investigation is a nanocrystalline metal whose grain size is below the critical size.

The positron lifetime distribution curves of both specimens are shown in Fig. 2, where τ_1 (150–200 ps), τ_2 (400–450 ps), and τ_3 (2000–2500 ps) are the peaks of positron lifetime. These positron lifetime peaks correspond to the occurrence of positron annihilation at one-atom-sized (or smaller) vacancies, at vacancy clusters, and at nanosized voids,[32,33] respectively. In the present paper, the intensities of τ_1, τ_2, and τ_3 are denoted I_1, I_2, and I_3, respectively. I_1 was the strongest of the three intensities, and both I_1 and I_2 of specimen B were stronger than those of specimen A. Note that the I_1 of specimen B was about twice as strong as that of specimen A, where I_1 is the intensity of one-atom or smaller-sized vacancies. It is known from an experiment[33] and a MD simulation[21] that vacancies exist in grain boundaries in nanocrystalline metals. The point defect formation energy in the grain boundary is lower than that in the lattice because vacancies are more stable in the grain boundary than in the lattice.[34] Therefore, it is suggested that specimen B contains more one-atom or smaller-sized vacancies in grain boundaries than specimen A, although the reason for an increase in vacancies by annealing is unknown. Also, Fig. 2 reveals that I_3 was much weaker than I_1 and I_2 for both specimens, where I_3 is the intensity of nanosized voids. This is in agreement with the HRTEM result that both specimens had no nanosized pores.

3.2 Tensile tests

The yield stresses for specimens A and B are shown in Fig. 3(a), where a filled circle is an average of yield stress. The yield stresses of specimen A were higher than those of specimen B. The fracture stresses for specimens A and B are

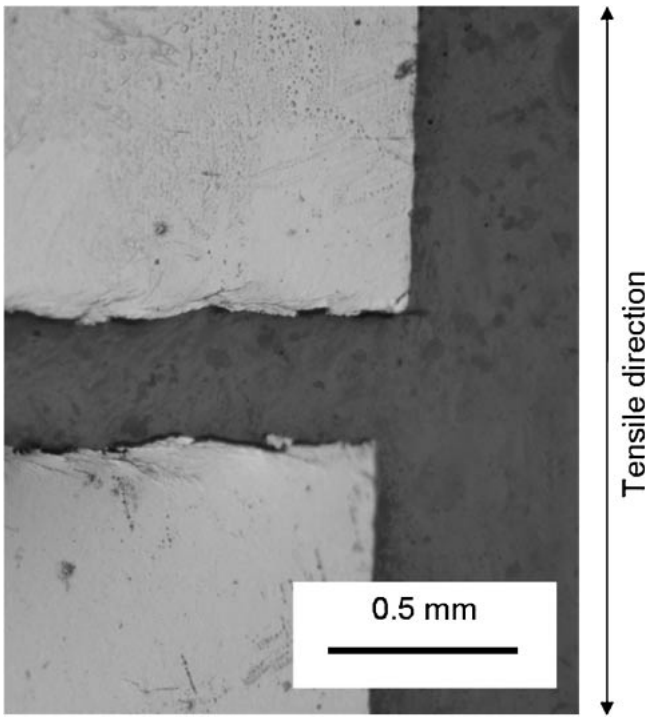

Fig. 4 Specimen A after the tensile test.

shown in Fig. 3(b), where a filled circle is an average of fracture stress. The fracture stresses of specimen A were higher than those of specimen B as in the case of yield stress. The plastic elongations to failure were much lower than 1% for both specimens. The same trend was reported in a previous work.[35] Thus, tensile ductility was very poor in the nanocrystalline Ni produced by electrodeposition.

The tensile tests showed that the yield and fracture stresses for specimen B containing more vacancies were lower than those for specimen A containing fewer vacancies. It was found from the HRTEM and PLM results that the difference in grain size between specimen A and specimen B was minor, and that the difference in microstructure between both specimens was in the number of one-atom-sized vacancies; that is, specimen A contained fewer vacancies than specimen B. On the other hand, significant internal stress relaxation hardly occurs during annealing.[18] Therefore, it is conclusively demonstrated that the yield and fracture stresses are decreased owing to the presence of one-atom-sized vacancies in the nanocrystalline Ni whose grain size is below the critical size.

Figure 4 shows the specimen A deformed to fracture. In general, a conventional metal is fractured with localized necking or fractured in a direction of 45 degrees with respect to the tensile direction. Also, an amorphous metal is fractured with shear bands, which are evidence of local deformation.[36] As shown in Fig. 4, however, the nanocrystalline Ni was fractured in a direction perpendicular to the tensile direction without localized necking and shear bands, suggesting that the fracture mechanism of the nanocrystalline Ni is different from those of conventional metals and amorphous metals. The brittle fracture mode of the nanocrystalline Ni is in agreement with the tensile test result that the elongation to failure was very low.

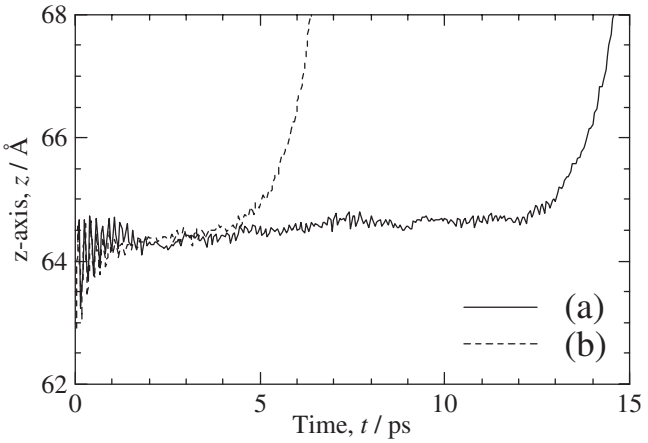

Fig. 5 The z-axis length versus time curves for the normal cell unit (a) and the vacancy-rich cell unit (b) calculated by the MD creep test simulations.

3.3 Molecular dynamics simulations

Figure 5 shows the z-axis length versus time curves for the normal cell unit (a) and the vacancy-rich cell unit (b) obtained from the MD creep test simulation. The minimum creep rate of each cell unit was calculated from the plastic deformation region of the z-axis length versus time curve, where the minimum creep rate is defined as the minimum slope during plastic deformation. As a result, the minimum strain rate was $7.8 \times 10^9\,s^{-1}$ for the normal cell unit and $1.9 \times 10^{10}\,s^{-1}$ for the vacancy-rich cell unit, respectively. Note that the minimum creep rate for the vacancy-rich cell unit was more than twice that for the normal cell unit. This indicates that grain boundary deformation is enhanced by vacancies in grain boundaries.

As shown in Fig. 5, the z-axis length increased rapidly at a certain time. In the creep simulations, no dislocation activity in the grains was found and deformation was due to movement of grain boundary atoms in both the normal and vacancy-rich cells. Thus, the sudden increase in strain rate is related to initiation of fracture. Inspection of Fig. 5 reveals that fracture was initiated in a shorter time for the vacancy-rich cell unit than that for the normal cell unit under the same stress, indicating that the fracture strength of the former is lower than that of the latter. This is in agreement with the experimental result.

Snapshots of the normal unit cell and vacancy-rich cell units at the onset of fracture are shown in Fig. 6. It can be seen that fracture is initiated from grain boundaries in both units. However, there was difference in location and development of cracks between both units. It is reported that for a nanocrystalline metal, vacancies in the grain boundary are created during its deformation and cracks are generated by joining these vacancies; finally, fracture occurs at the grain boundary due to the cracks.[37] It is therefore suggested that the formation of cracks is enhanced by the presence of more vacancies in grain boundaries.

Figure 7 shows the stress-strain curves for the normal cell and vacancy-rich cell units obtained from compression test simulations. It can be seen that the yielding phenomenon, that is, an apparent plastic deformation, occurs around $\varepsilon = 7\%$ after a large strain. The relative configuration of almost all atoms did not change by loading and unloading in the strain

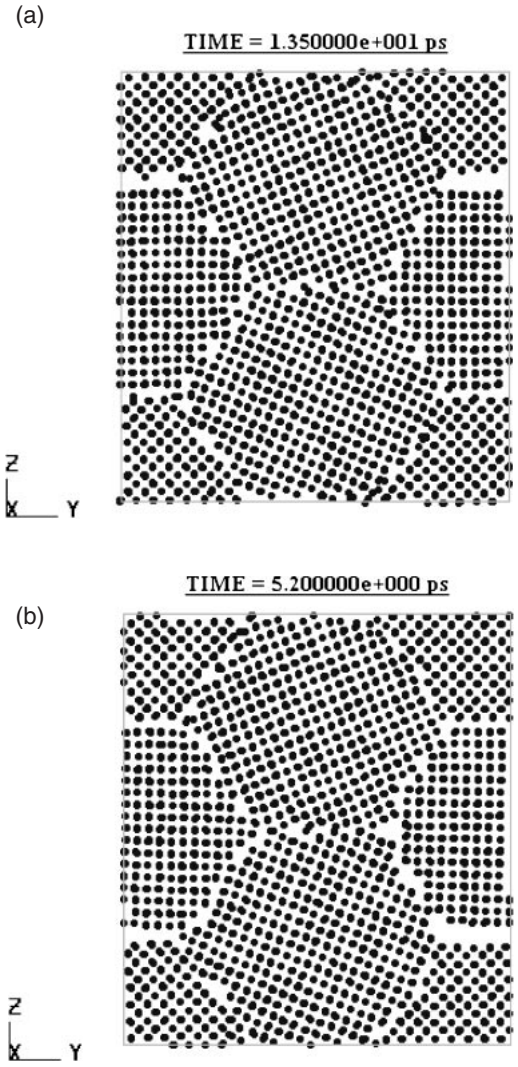

Fig. 6 Snapshots during the creep test simulation, (a) the normal cell unit at 13.5 ps and (b) the vacancy-rich cell unit at 5.2 ps.

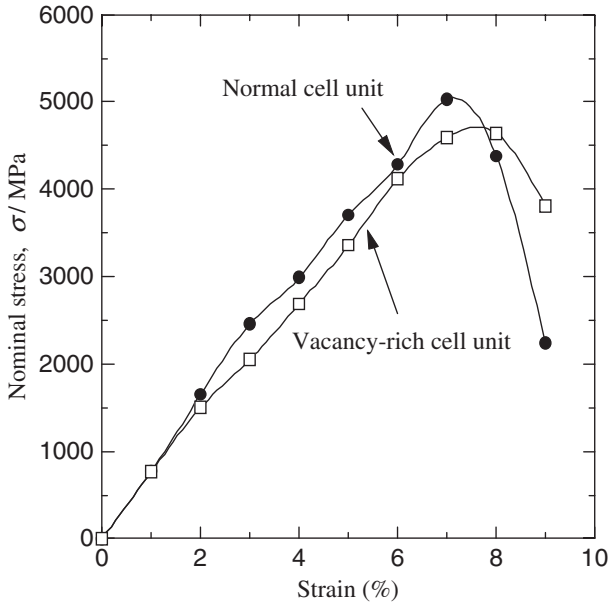

Fig. 7 Stress-strain curves for the normal cell and vacancy-rich cell units obtained by performing the MD compression tests.

range of $\varepsilon < 7\%$, indicating that the strain range of $\varepsilon < 7\%$ is an elastic deformation region. The same trend of a large elastic deformation region has been reported in the previous work on the basis of MD simulation.[38] In reality, the elastic strain is less than 0.1–0.2%. The reason for the large elastic strain obtained in the MD simulations is unknown. As shown in Fig. 7, the yield stress for the normal cell unit was about 8% higher than that for the vacancy-rich cell unit. Also, the flow stress was drastically decreased after yielding ($\varepsilon = 7\%$) for the normal cell unit; however, for the vacancy-rich cell unit, the flow stress was gradually increased from $\varepsilon = 7\%$ to 8% after yielding and then gradually decreased from $\varepsilon = 8\%$. Also, it appears that the tilt of a line in an elastic region for the normal cell unit is a little larger than that for the vacancy-rich cell unit, suggesting that the elastic modulus is reduced by the presence of vacancies in the grain boundary. Thus, the grain boundary defects affected the deformation characteristics of a nanocrystalline Ni.

4. Discussion

The plastic deformation of a nanocrystalline metal is a result of an interplay between the sliding of atomic planes and atomic shuffling across the grain boundary, and the vacancy in the grain boundaries is the driving force for atomic shuffling.[39] Hasnaoui *et al.*[18] showed from MD simulation that a grain boundary disorder sample exhibits a larger stain rate than a sample with less disorder because the disorder in the grain boundary affects the atomic movement. This is in agreement with the present investigation that the mechanical properties of the nanocrystalline Ni are affected by the disorder of the grain boundary due to the presence of vacancies. In addition, the present experimental and simulation results suggested that vacancies in the grain boundary affect not only the deformation, but also the fracture in a nanocrystalline metal. Brittleness depends on the difference in internal energy between the grain interior and the grain boundary when fracture is initiated at the grain boundary; hence, fracture tends to occur at the grain boundary when the grain boundary energy is high.[33] The grain boundary energy, E_{gb}, can be given by[40]

$$E_{gb} = (E - E_0)/S_{gb} \tag{2}$$

where E is the internal energy of the cell, E_0 is the internal energy of a perfect crystal whose number of atoms is the same as that of the cell, and S_{gb} is the grain boundary dimensions of the cell. The grain boundary energies prior to deformation for the normal cell and vacancy-rich cell units were 1.71 and 1.79 J/m^2, respectively. These grain boundary energy values are a little larger than that in the previous literature,[41] but they seems reasonable, considering the specific cell unit consisting of four columnar, uniform hexagonal fcc grains rotated around the [100] axis. Note that the grain boundary energy of the vacancy-rich cell unit is higher than that of the normal cell unit. This is because the vacancies affect the grain boundary structure.[34] Therefore, it is suggested that the grain boundary energy increases owing to the presence of vacancies in the grain boundary, resulting in the enhancement of crack formation at the grain boundary.

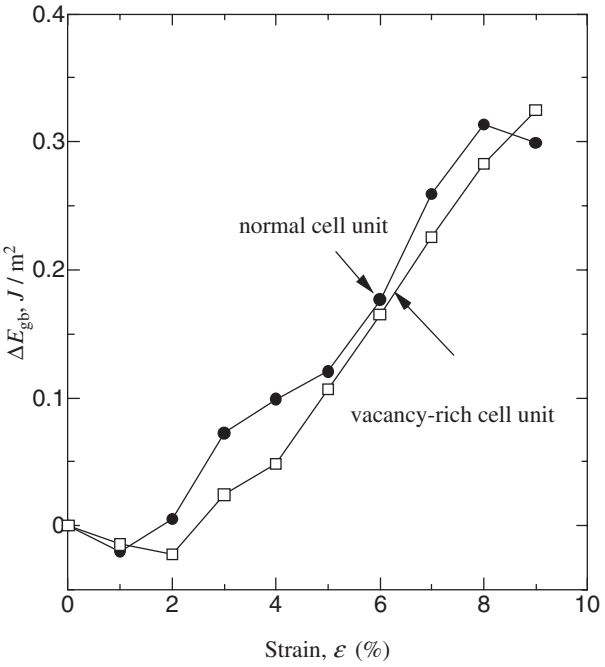

Fig. 8 Variation in grain boundary energy (ΔE_{gb}) with strain for the normal cell and vacancy-rich cell units.

Vacancies effectively migrate to a more convenient position and reduce the grain boundary energy during grain boundary sliding.[42] Molteni *et al.*[43] showed that vacancies in the grain boundary affect the variation in grain boundary energy during grain boundary sliding. Hence, the effect of vacancies on deformability in a nanocrystalline metal may be explained on the basis of the variation of the grain boundary energy with straining. Figure 8 shows the variation in grain boundary energy with strain for the normal cell and vacancy-rich cell units. Note that the variation in grain boundary energy for the vacancy-rich cell unit is lower than that for the normal cell unit before yielding. Inspection of Figs. 7 and 8 reveals that the variation of the flow stress with strain corresponds to the variation of the grain boundary energy with strain, except an initial stage of elastic deformation where the grain boundary energy decreases with strain. A decrease in grain boundary energy with strain in an initial stage of elastic deformation may result from a decrease in free volumes in the grain boundaries due to the compressive deformation. Sansoz and Molinari[44] noted that while a high grain boundary energy seems necessary for triggering grain boundary sliding, the grain boundary energy is not a sufficient parameter. It can be seen from Fig. 8 that not only the grain boundary energy, but also the variation in grain boundary energy with straining is important for grain boundary deformation. Atomic shuffling plays an important role in the accommodation of grain boundary deformation.[39] Therefore, it is suggested that at the onset of plastic deformation, because the movement of atoms such as atomic shuffling during grain boundary sliding is enhanced by the presence of vacancies in the grain boundary, the vacancies in the grain boundary reduce the variation in grain boundary energy with strain.

5. Conclusions

The effects of vacancies on the deformation characteristics of nanocrystalline nickel were investigated by conducting tensile tests and MD simulations.

In the experiments, the yield stress and fracture stress for the nanocrystalline Ni containing more vacancies were lower than those for the one containing fewer vacancies.

The MD simulations showed that the grain boundary energy is increased by the presence of vacancies in the grain boundary. Therefore, an increase in grain boundary energy due to vacancies in the grain boundary is suggested to enhance grain boundary fracture. Also, the MD simulations indicated that because an increase in grain boundary energy with straining is reduced by the presence of vacancies in the grain boundary, the vacancies make a nanocrystalline metal deformable.

REFERENCES

1) R. Birringer: Mater. Sci. Eng. A **117** (1989) 33–43.
2) H. Gleiter: Acta Mater. **48** (2000) 1–29.
3) K. S. Kumar, H. Van Swygenhoven and S. Suresh: Acta Mater. **51** (2003) 5743–5774.
4) S. C. Tjong and H. Chen: Mater. Sci. Eng. R **45** (2004) 1–88.
5) D. Wolf, V. Yamakov, S. R. Phillpoc, A. Mukherjee and H. Gleiter: Acta Mater. **53** (2005) 1–40.
6) M. A. Meyers, A. Mishra and D. J. Benson: Prog. Mater. Sci. **51** (2006) 427–556.
7) E. O. Hall: Proc. Phys. Soc. B **64** (1951) 747–753.
8) N. J. Petch: J. Iron Steel Inst. **174** (1953) 25–31.
9) A. H. Chokshi, A. Rosen, J. Karch and H. Gleiter: Scripta Mater. **23** (1989) 1679–1684.
10) T. G. Nieh and J. Wadsworth: Scripta Metall. Mater. **25** (1991) 955–958.
11) G. E. Fougere, J. R. Weertman, R. W. Siegel and S. Kim: Scripta Metall. Mater. **26** (1992) 1879–1883.
12) C. A. Schuh, T. G. Nieh and H. Iwasaki: Acta Mater. **51** (2003) 431–443.
13) C. C. Koch: Scripta Mater. **49** (2003) 657–662.
14) J. Schiøtz, F. Dalla Torre and K. W. Jacobsen: Nature **391** (1998) 561–563.
15) H. Van Swygenhoven and P. M. Derlet: Phys. Rev. B **64** (2001) 224105(1)-(9).
16) V. Yamakov, D. Wolf, S. R. Phillpot, A. K. Mukherjee and H. Gleiter: Nature Mater. **3** (2004) 43–47.
17) J. Schiøtz, T. Vegge, F. Dalla Torre and K. W. Jacobsen: Phys. Rev. B **60** (1999) 11971–11983.
18) A. Hasnaoui, H. Van Swygenhoven and P. M. Derlet: Acta Mater. **50** (2002) 3927–3939.
19) T. Shimokawa, A. Nakatani and H. Kitagawa: JSME Int. J., Ser. A **47** (2004) 83–91.
20) Y. Fukai, M. Mizutani, S. Yokota, M. Kanazawa, Y. Miura and Y. Watanabe: J. Alloy Comp. **356–357** (2003) 270–273.
21) H. Van Swygenhoven, M. Spaczer, A. Caro and D. Farkas: Phys. Rev. B **60** (1999) 22–25.
22) H. Van Swygenhoven and P. M. Derlet: Phys. Rev. B **64** (2001) 224105(1)-(9).
23) P. Ballo, N. Kioussis and G. Lu: Phys. Rev. B **64** (2001) 024104(1)-(7).
24) M. Legros, B. R. Elliott, M. N. Rittner, J. R. Weertman and K. J. Hemker: Philos. Mag. A **80** (2000) 1017–1026.
25) M. J. Puska and R. M. Nieminen: J. Phys. F: Met. Phys. **13** (1983) 333–346.
26) D. Farkas and W. A. Curtin: Mater. Sci. Eng. A **412** (2005) 316–322.
27) Z. Chen and J. Ding: Nanostruct. Mater. **10** (2003) 205–215.
28) V. Yamakov, D. Wolf, M. Salazar, S. R. Phillpot and H. Gleiter: Acta Mater. **49** (2001) 2713–2722.
29) T. Shimokawa, A. Nakatani and H. Kitagawa: Phys. Rev. B **71** (2005)

224110(1)-(8).
30) P. M. Derlet and H. Van Swygenhoven: Scripta Mater. **47** (2002) 719–724.
31) V. Rosato, M. Guillope and B. Legrand: Philos. Mag. A **59** (1989) 321–336.
32) I. K. MacKenzie: *Positron Solid-State Physics*, (North-Holland Publishing Company, Amsterdam, 1983) pp. 196.
33) S. Van Petegem, F. Dalla Torre, D. Segers and H. Van Swygenhoven: Scripta Mater. **48** (2003) 17–22.
34) A. Suzuki and Y. Mishin: Interface Sci. **11** (2003) 131–148.
35) T. Yamasaki: Scripta Mater. **44** (2001) 1497–1502.
36) P. S. Steif, F. Spaepen and J. W. Hutchinson: Acta Metallur. **30** (1982) 447–455.
37) D. Farkas, H. Van Swygenhoven and P. M. Darlet: Phys. Rev. B **66** (2002) 060101(1)-(4).
38) A. C. Lund, T. G. Nigh and C. A. Schuh: Phys. Rev. B **69** (2004) 012101(1)-(4).
39) H. Van Swygenhoven, P. M. Derlet and A. Hasnaoui: Phys. Rev. B **66** (2002) 24101(1)-(8).
40) N. Tanaka, K. Ikeda, F. Yoshida, H. Nakashima and H. Abe: J. Japan Inst. Metals **68** (2004) 240–246.
41) S. P. Chen, D. J. Srolovitz and A. F. Voter: J. Mater. Res. **4** (1989) 62–77.
42) P. Ballo, J. Degmova and V. Slugen: Phys. Rev. B **72** (2005) 064118(1)-(5).
43) C. Molteni, N. Marzari, M. C. Payne and V. Heine: Phys. Rev. Lett. **79** (1997) 869–872.
44) F. Sansoz and J. F. Molinari: Acta Mater. **53** (2005) 1931–1944.